EJNMMI Physics

ORIGINAL RESEARCH Open Access

Towards personalised dosimetry in patients with liver malignancy treated with ^{90}Y-SIRT using in vivo-driven radiobiological parameters

Yaser H. Gholami[1,2,3*], Kathy P. Willowson[3] and Dale L. Bailey[1,2,3*]

*Correspondence: yaser.gholami@sydney.edu.au; dale.bailey@sydney.edu.au

[1] Faculty of Medicine and Health, The University of Sydney, Sydney, Australia
[2] Sydney Vital Translational Cancer Research Centre, University of Sydney, Sydney, Australia
[3] Department of Nuclear Medicine, Royal North Shore Hospital, Sydney, Australia

Abstract

Background: The prediction of response is one of the major challenges in radiation-based therapies. Although the selection of accurate linear–quadratic model parameters is essential for the estimation of radiation response and treatment outcome, there is a limited knowledge about these radiobiological parameters for liver tumours using radionuclide treatments.

Methods: The "clinical radiobiological" parameters (T_p, T_k, α, α/β) for twenty-five patients were derived using the generalised linear–quadratic model, the diagnostic ([^{18}F] FDG PET/CT) and therapeutic ([^{90}Y]-SIR-Spheres PET/CT) images to compute the biological effective dose and tumour control probability (TCP) for each patient.

Results: It was estimated that the values for α and α/β parameters range in $\approx$ 0.001–1 Gy^{-1} and $\approx$ 1–49 Gy, respectively. We have demonstrated that the time factors, T_p, T_k and T_{critic} are the key parameters when evaluating liver malignancy lesional response to [^{90}Y]SIR-Spheres treatment. Patients with cholangiocarcinoma have been shown to have the longest average T_p ($\approx 236 \pm 67$ d), highest TCP ($\approx 53 \pm 17\%$) and total liver lesion glycolysis response ($\Delta TLG_{liver} \approx 64\%$), while patients with metastatic colorectal cancer tumours have the shortest average T_p ($\approx 129 \pm 19$ d), lowest TCP ($\approx 28 \pm 13\%$) and $\Delta TLG_{liver} \approx 8\%$, respectively.

Conclusions: Tumours with shorter T_k have shown a shorter T_{critic} and thus poorer TCP and ΔTLG_{liver}. Therefore, these results suggest for such tumours the [^{90}Y]SIR-Spheres will be only effective at higher initial dose rate (e.g. >50 Gy/day).

Keywords: ^{90}Y, Radioembolisation, SIRT, Dose, Response

Background

Selective internal radionuclide therapy (SIRT) with yttrium-90 [^{90}Y]-microspheres (SIR-Spheres; Sirtex, Sydney, Australia) (^{90}Y-SIRT) has been used as a locoregional therapy for liver metastases of malignancies including neuroendocrine tumours (NETs) and colorectal cancer (CRC) [1, 2], advanced hepatocellular carcinoma (HCC) [3–6] and intrahepatic cholangiocarcinoma (ICC) [7–9]. Although SIRT is a well-established radionuclide therapy (RNT) platform, there are ongoing efforts to further improve treatment planning using personalised dosimetry [10]. The primary principle

of radiation therapy is to be able to accurately plan and deliver effective doses to the tumour while minimising the dose to healthy tissues. Knowing the true absorbed dose to tissue compartments is the primary way to safely individualise therapy for maximal response while respecting normal tissue tolerances. Recent progress in positron emission tomography (PET)/computed tomography (CT) imaging has improved the ability to estimate absorbed ^{90}Y doses and achieve a more accurate dosimetric approach to the activity calculation in ^{90}Y-SIRT [11–14].

Furthermore, one of the major challenges in radiation therapy (both RNT and external beam radiotherapy, EBRT) is to predict the radiobiological response from a particular dose delivered to a tumour [15, 16]. Amongst the established radiobiological models, the linear–quadratic (LQ) model has been best validated by experimental and clinical data and is commonly used to analyse both in vitro and in vivo clinical dose response [17, 18]. In addition to considering the effects of cellular lethal (i.e. DNA double-strand break, DSB) and sub-lethal damage by radiation, the generalised LQ model (GLQ) also includes the effect of the dose rate and the cell proliferation effects [19–21]. Clinically, the GLQ model is increasingly used to predict tumour control probability (TCP) [19–21].

In previous studies [22, 23], we have demonstrated that an in vitro metabolic assay and in vivo metabolic imaging (i.e. Fluorine-18 [^{18}F]-fluorodeoxyglucose PET imaging (FDG PET) can be used to derive radiobiological parameters and assess the prognostic factors for radioembolisation of liver metastases from colorectal cancer. Furthermore, our in vitro study demonstrated that dose rate variation can significantly impact the ^{90}Y-SIRT dose response. Since the initial dose rate decreases exponentially over time, at a critical time (T_{critic}) or critical dose rate (R_{critic}) the DNA damage (the probability of causing DSBs) effectively becomes insignificant [23] due to the rate of DNA repair. Both T_{critic} and R_{critic} are obtained based on the α parameter (radiosensitivity of the tumour cell), the radionuclide half-life, initial dose rate, and the cell repopulation time (T_{p}) [23]. The other key radiobiological parameter that adversely affects the local tumour control and/or survival is the 'kick-off' time (T_{k}) [24]. Previous studies have shown that for certain cancer types (particularly highly proliferating cancers with T_{p} ranging from a few days to a few weeks) there exists a short period of time after the start of radiotherapy before the tumour starts to grow more rapidly than prior to irradiation [24–28] and this is referred to as the 'kick-off time'. Since the dose rate in RNT is mono-or bi-exponentially decreasing and the treatment time is usually long (*e.g.* weeks to months), the T_{k} can significantly impact the biological effective dose (BED) and treatment outcome (e.g. tumour control probability, TCP) [24].

The prediction of response is one of the major challenges in radiation-based therapies. Although the selection of accurate LQ parameters for T_{p}, T_{k}, α, and α/β is pivotal for a reliable estimate of radiation response and treatment outcome, there is a limited knowledge about these radiobiological parameters for liver tumours [29]. To obtain accurate dosimetry and tumour response prediction for ^{90}Y-SIRT, personalised characterisation of the individual patient's radiobiological parameters is required. Therefore, the aim of this study was to develop a model to fit clinical tumour survival fraction data from treated patients with liver malignancy to derive the radiobiological parameters, evaluate the dosimetry and the treatment outcome specific to each patient.

Methods

Overview

The clinical radiobiological parameters (i.e. T_p, T_k, α, α/β) for twenty-five patients were derived using the diagnostic (FDG PET/CT) and therapeutic (^{90}Y-SIRT PET/CT) images to compute the BED map, TCP and FDG PET total liver lesion glycolysis (TLG) for each patient. Furthermore, the relationship between the radiobiological parameters and the calculated dosimetric quantities was investigated.

Patient characteristics

The data for twenty-five patients with liver malignancy including pancreatic neuroendocrine tumours (PNET), colorectal cancer (CRC), pancreatic ductal adenocarcinoma (PDAC), small bowel neuroendocrine tumours (SBNET), hepatocellular carcinoma (HCC), neuroendocrine Carcinoma (NEC) and other metastatic tumours who were treated with [^{90}Y]-SIR-Spheres between July 2019 and April 2021 were used in this study. All patients gave informed consent at the time of the procedure for their clinical and image data to be used for further research, education, training, and audit. For each patient a complete imaging set suitable for lesional analysis was available. Similar to our previous study [22], an individual imaging set consisted of baseline FDG PET/CT (acquired $\leq$ 28 days prior to radioembolisation), ^{90}Y-SIRT PET/CT (acquired within 24 h of radioembolisation), and follow-up FDG PET/CT (acquired $\leq$ 80 days post-radioembolisation). Treatment time is the time interval between the baseline and follow-up FDG, and each patient's treatment time is listed in Table 1. All patients underwent pre-treatment interventional arterial mapping and abdominal Technetium-99 m macroaggregated albumin ([^{99m}Tc]MAA) single-photon emission computed tomography SPECT/CT imaging prior to treatment to assess the lung shunt fraction and possible extrahepatic uptake to determine the feasibility, safety, and number of injections required for selective treatments.

Image analysis

All imaging data were acquired using similar scanners and protocols that were used in our previous study [22]. Images were acquired on a Siemens Biograph mCT-S (64) PET/CT system (Knoxville, TN, USA) with 550 picosecond timing resolution time-of-flight (ToF) capabilities, an axial field of view of 21.8 cm and 78 cm crystal ring diameter. Images (with voxel size = $4.072 \times 4.072 \times 2$ mm) were reconstructed using the standard OSEM (with 3 iterations and 21 subsets) reconstruction method in conjunction with ToF modelling and point spread function recovery. Our 'low-dose protocol' (i.e. as two 10 min frames over the liver and reconstructed with 3i21s and a 5 mm Gaussian filter) was used to acquire baseline and follow-up PET/CT data. The quantitative liver ^{90}Y PET/CT data were reconstructed with 1i21s with no filtering. Siemens' Intevo-6 or Symbia.T16 were used to acquire the MAA planning SPECT/CT data with low energy parallel hole collimators and standard CT-based attenuation correction were used for reconstruction. To avoid breakdown of the ^{99m}Tc-MAA in vivo, in all cases acquisition was performed within 1 h following implantation. The [^{90}Y]-microsphere dosimetry

Table 1 Summary of estimated radiobiological parameters

Cancer type	T_t (days)	T_p (days)	T_k (d)	α (Gy^{-1})	α/β (Gy)
Breast	49	124	23	0.009	5.00
PNET	47	166	22	0.009	11.2
Adrenocortical carcinoma	49	136	9.0	0.005	4.21
CRC	53	170	26	0.005	49.8
Cholangiocarcinoma	42	200	41	0.015	1.00
CRC	42	108	2.0	0.006	5.83
CRC	49	180	29	0.008	4.00
Rectal adenocarcinoma	46	300	27	0.200	5.91
Cholangiocarcinoma	48	348	48	0.100	1.53
CRC	47	87.0	10	0.010	6.45
Cholangiocarcinoma	47	59.0	1.0	0.001	5.98
Cholangiocarcinoma	48	336	23	0.050	1.00
Sigmoid adenocarcinoma	77	232	27	0.200	6.67
Breast	55	180	55	0.080	1.00
Prostate	56	250	56	0.100	2.00
CRC	56	97.0	50	0.030	4.29
PNET	23	134	49	1.000	2.20
PDAC	49	180	49	0.300	1.00
SBNET	59	300	59	0.800	8.89
Mesothelioma	56	157	39	0.010	8.13
PNET	48	200	48	0.124	12.4
HCC	50	90.0	10	0.003	2.78
Oesophageal	47	200	46	0.050	1.25
SBNET	54	86.0	13	0.022	11.1
NEC	41	87.0	1.0	0.028	1.40

T_t, treatment time; T_p, cell repopulation time; T_k, kick-off time; *PNET* pancreatic neuroendocrine tumours, *CRC* colorectal cancer, *PDAC* pancreatic ductal adenocarcinoma, *SBNET* small bowel neuroendocrine tumours, *HCC* hepatocellular carcinoma, *NEC* neuroendocrine carcinoma.

navigator software (RapidSphere®) within a commercial platform (Velocity, Varian Medical Systems, Palo Alto, USA) was used to analyse the patient images including the absorbed dose. The absorbed dose was calculated using the local deposition method [30–32].

The ^{90}Y-SIRT PET/CT images were first registered to the pre- and post-implantation FDG PET/CT images using the deformable image registration package provided. The Velocity deformable registration algorithm applies multiresolution free-form deformations and an intensity-based B-spline multipass algorithm to provide a high-level deformable image registration accuracy [32, 33]. The deformable registration provided a one-to-one correlation between voxels on different images and time points, allowing for mapping of anatomical data and structure sets from [^{90}Y]-microsphere PET/CT, pre-treatment FDG PET/CT to follow-up FDG PET/CT.

Dose and BED calculations

Dose and survival fraction

The ^{90}Y dosimetry navigator was used to calculate the lesion absorbed dose distribution from the ^{90}Y PET/CT images. Next, the dose and the normalised standard uptake value (SUV) Volume Histogram of the ^{90}Y PET/CT and registered pre- and post-treatment

FDG images were computed and imported into MATLAB (R2020a) software. In our previous in vitro study [23], it was demonstrated that the measured radiation survival by metabolic cell assay is comparable to that of clonogenic assays. Additionally, the metabolic assay measures all viable cells thus representing cells from a true tumour population rather than just clonogenic cells [34, 35]. The FDG scan uses a glucose analogue and is the most commonly used PET tracer to assess tumour metabolism. Due to increased glucose metabolism in most types of tumours, the FDG PET is widely used clinically for tumour imaging [36]. The FDG uptake in PET imaging is a measure of the tissue glucose metabolism and is usually high in high-grade tumours (e.g. maximum SUV = 11) and relatively low in low-grade (e.g. maximum SUV = 7) tumours [37]. Additionally, in our previous study [23] we demonstrated that in vivo metabolic imaging such as FDG PET can be used to assess the metabolic dose response as well as prognostic factors for radioembolisation of liver metastases from colorectal cancer. Furthermore, the change in tumour voxel SUV ratio at a specific dose level from a serial FDG PET/CT imaging (i.e. pre- and post-treatment FDG images) can be used to model the tumour voxel dose response [38]. In this study, similarly we have proposed that the ratio of voxel SUV from pre- and post-treatment FDG images should represent the metabolic radiation survival fraction (SF) due to [^{90}Y]-microspheres irradiation. Therefore, the ratio of voxel SUV from pre- and post-treatment should represent the metabolic radiation survival fraction (SF) due to [^{90}Y]-microspheres irradiation. In addition, to account for dose heterogeneity the SF is calculated based on the dose volume histogram (DVH) by:

$$\mathrm{SF} = \sum_i \frac{V_i}{V_0} \mathrm{SF}(D_i) \tag{1}$$

$$\mathrm{SF}(D_i) = \frac{\mathrm{SUV}_{i,\mathrm{post-FDG}}}{\mathrm{SUV}_{i,\mathrm{pre-FDG}}} \tag{2}$$

where V_0 is the tumour volume and V_i is the sub volume corresponding to ^{90}Y dose bin D_i on the DVH. Hence using Eqs. 1 and 2, the survival fraction of cancer cells in a tumour volume with an initial volume of V_0 can be estimated by computing the ratio of voxel SUV from pre- and post-treatment FDG images. Next, the voxel SF (VSF) data was fitted to the GLQ model (Eq. 3, using MATLAB software) to estimate the radiobiological parameters, T_p, T_k, α, α/β. The GLQ fit is commonly used in the field of radiobiology to derive radiobiological parameters both in vitro and in vivo studies [16].

$$\mathrm{SF} = e^{-\left(\alpha D + G\beta D^2 + \gamma\left(T_\mathrm{t} - T_\mathrm{k}\right)\right)} \tag{3}$$

$$\mathrm{SF} = e^{-\left(\alpha D + G\beta D^2 - \frac{T_{1/2}}{T_\mathrm{p}}\left(\frac{\ln(2)}{\alpha R_0 T_\mathrm{p}}\right) - \left(\frac{\ln(2) T_\mathrm{k}}{T_\mathrm{p}}\right)\right)} \tag{4}$$

$$G = \frac{2}{D^2} \int_{-\infty}^{\infty} \dot{D}(t)\mathrm{d}t \int_{-\infty}^{t} \dot{D}'\left(t'\right) e^{-\mu\left(t-t'\right)} \mathrm{d}t' \tag{5}$$

For further personalisation of the GLQ, the treatment time (T_t) was considered to be equal to the critical time (T_critic) to include the effect of initial dose rate used for each treatment [23]:

$$T_{\mathrm{t}} = T_{\mathrm{critic}} = \frac{T_{1/2}}{\ln(2)} \ln\left(\frac{\ln(2)}{\alpha R_0 T_{\mathrm{p}}}\right) \tag{6}$$

where $T_{1/2}$ is the ^{90}Y half-life (i.e. $\approx$ 2.7 days), α is the cell radiosensitivity, R_0 is the initial does rate, and T_{p} is the tumour cell proliferation (or repopulation) time. Hence by replacing the T_{t} with T_{critic} and also substituting the tumour cell proliferation (or repopulation) constant, $\gamma = \ln(2)/T_{\mathrm{p}}$, in Eq. 4 we can obtain T_p, T_{k}, α, α/β parameters. Furthermore, the GLQ model includes the G-factor (or the Lea–Catcheside factor described by Eq. 5) to account for the kinetics of DNA strand break damage and repair in obtaining the true fraction of surviving cells in an irradiated cell population within the tumour [23]. In Eq. 5, the first integral represents the physical absorbed dose. The integrand of the second integral over t' refers to the first DNA single-strand break (SSB) of two SSBs needed to cause lethal DNA double-strand (DSB) damage. Also, the integral over t refers to the second SSB of remaining of two SSBs to cause a DSB. The exponential term reflects the repair and therefore reduction in induction of 2 SSB$\rightarrow$DSB process due to decreasing dose rate [23]. Also, μ (which is $\ln(2)/T_{\mathrm{rep}}$) is the DNA repair time constant (T_{rep} is the DNA repair half-life which is $\approx$ 1.5 hr [23]).

The R_{critic} was also calculated by Eq. 7 for further assessment of the treatment outcome.

$$R_{\mathrm{critic}} = \frac{\ln(2)}{\alpha T_{\mathrm{p}}} \tag{7}$$

Both T_{critic} and R_{critic} were calculated theoretically using Eqs. 6 and 7 for a range of α, T_{p} and R_0 shown in Fig. 5a–b and using the clinically driven radiobiological parameters for comparison. Furthermore, to show the impact of the proliferation acceleration on dose rate efficiency during the treatment time, the $R_{\mathrm{critic}(k)}$ was also calculated for when the $T_{\mathrm{p}} \approx T_{\mathrm{k}}$ (this can represent the highest acceleration in tumour proliferation rate).

BED calculation

The computed lesion dose for each patient was used as an input to generate the lesion BED map. The BED calculations were performed considering the following methods:

Method1. Due to low dose rate and relatively long treatment time (^{90}Y half-life $\approx$ 2.7 days), repair of sub-lethal damage might take place during the treatment duration. Additionally, highly proliferating cancers can have short T_{k} (relative to the treatment time) which could impact the survival fraction and TCP. Therefore, treatment with an exponentially decaying source (integrated to fixed treatment time, T) and considering the above parameters can be computed as (Method 1):

$$\mathrm{BED}_{\mathrm{exp}} = D \times \mathrm{RE} - \frac{\ln(2)(T - T_{\mathrm{k}})}{\alpha T_{\mathrm{p}}} \tag{8}$$

$$\mathrm{RE} = 1 + \left(\frac{2R_0\lambda}{\mu - \lambda}\right)\left(\frac{\beta}{\alpha}\right)\left(\frac{\frac{1}{2\lambda}\left(1 - e^{-2\lambda T}\right) - \frac{1}{\mu+\lambda}\left(1 - e^{-(\mu+\lambda)T}\right)}{1 - e^{-\lambda T}}\right) \tag{9}$$

$$R_0 = \frac{\lambda D}{1 - e^{-\lambda T}} \tag{10}$$

Method 2. This method is the simplified version of Method 1 where treatment time is integrated to $T \to \infty$. This is the standard BED formulation [39] in the radionuclide therapy dosimetry to calculate the BED:

$$\mathrm{BED}_\infty = D.\mathrm{RE}_\infty \tag{11}$$

$$\mathrm{RE}_\infty = 1 + \left(\frac{R_0}{\mu + \lambda}\right)\left(\frac{\beta}{\alpha}\right) \tag{12}$$

TCP calculations

For each tumour with N voxels, the voxel TCP was calculated first and then the overall expected TCP of tumour was obtained as the product of the expected voxel TCP [40, 41]:

$$\mathrm{TCP}_{\mathrm{voxel}} = e^{-D_c V \cdot \mathrm{VSF}} \tag{13}$$

$$\mathrm{TCP} = \prod_{i=1}^{N} [\mathrm{TCP}_{\mathrm{voxel}}]^{\frac{1}{N}} \tag{14}$$

where D_c (i.e. 1×10^6) and V are the density of clonogens per cm^3 and the voxel volume respectively.

TLG calculations

Finally, the $\mathrm{TLG}_{\mathrm{liver}}$ of each liver lesion was calculated by multiplying the metabolic tumour volume of that lesion with its corresponding mean SUV and the $\Delta\mathrm{TLG}_{\mathrm{liver}}$ was calculated in percentage as [22]:

$$\Delta\mathrm{TLG}_{\mathrm{liver}}(\%) = \frac{\mathrm{TLG}_{\mathrm{pre}} - \mathrm{TLG}_{\mathrm{post}}}{\mathrm{TLG}_{\mathrm{pre}}} \times 100 \tag{15}$$

where $\mathrm{TLG}_{\mathrm{pre}}$ and $\mathrm{TLG}_{\mathrm{post}}$ are the $\mathrm{TLG}_{\mathrm{liver}}$ values based on pre- and post-treatment FDG PET images.

Results

A summary of the derived radiobiological parameters and dosimetry is presented in Tables 1, 2 and 3. The average T_p, T_k, α, α/β parameters were $\approx 176 \pm 16.3$ days, 30.6 ± 3.8 days, 0.10 ± 0.05 Gy^{-1} and 7 ± 2 Gy, respectively. The mean dose, BED_∞ , $\mathrm{BED}_{\mathrm{exp}}$, TCP and $\Delta\mathrm{TLG}_{\mathrm{liver}}$ were $\approx 63.6 \pm 14.2$ Gy, 97.8 ± 23.6 Gy, 61.6 ± 14.2 Gy, $43.5\% \pm 5.6\%$ and $45.2\% \pm 9.0\%$, respectively. For all the patients, the treatment time T_t is greater than or equal to T_k. Therefore, although there is a variation in the T_t, this does not influence the derivation of the other parameters [23].

Data presented in Table 4 are grouped by cancer type. Patients with breast and cholangiocarcinoma metastatic liver lesions have shown the highest TCP (i.e. 60%

Table 2 A list of estimated critical dose rate, R_{critic} and time, T_{critic}

Cancer type	R_{critic}(Gy/days)	$R_{critic(k)}$(Gy/days)	R_0(Gy/days)	T_{critic}(days)
Breast	0.620	3.32	12.3	12
PNET	0.465	3.45	13.1	13
Adrenocortical carcinoma	1.0	16.3	13.5	10
CRC	0.814	5.24	32.8	14
Cholangiocarcinoma	0.231	1.13	7.28	13
CRC	1.0	56.1	8.62	8
CRC	0.481	3.01	11.0	12
Rectal adenocarcinoma	0.012	0.13	3.18	22
Cholangiocarcinoma	0.02	0.14	8.82	23
CRC	0.777	6.76	8.59	9
Cholangiocarcinoma	11.7	693	70.5	7
Cholangiocarcinoma	0.041	0.60	10.2	21
Sigmoid adenocarcinoma	0.015	0.13	13.0	26
Breast	0.048	0.16	11.8	21
Prostate	0.028	0.12	8.65	22
mCRC	0.238	0.46	7.65	13
PNET	5.00×10^{-3}	0.01	11.0	30
PDAC	0.013	0.05	2.29	20
SBNET	0.003	0.02	59.8	38
Mesothelioma	0.442	1.76	15.5	14
PNET	0.028	0.12	25.4	26
HCC	3.070	26.5	20.9	7
Oesophageal	0.069	0.30	4.58	16
SBNET	0.362	2.36	12.9	14
NEC	0.284	22.4	4.44	11

R_{critic}, critical dose rate; $R_{critic(k)}$, critical dose rate considering the T_k; R_0, initial dose rate; T_{critic}, critical time.

and 53%, respectively) and ΔTLG_{liver} (66% and 63%, respectively). Furthermore, these patients have the longest repopulation time (mean $T_p \approx 235 \pm 67.2$ days). Also, patients with metastatic CRC (mCRC, with shortest mean $T_p \approx 128 \pm 19.4$ days) have shown the poorest TCP and ΔTLG_{liver}, 28.2% and 7.7%, respectively. Additionally, it was estimated that patients with mCRC liver lesions have the smallest α (i.e. 0.0100 ± 0.005) with shortest T_k (23.5 ± 8.3 days) and T_{critic} (i.e. $\approx 11.4 \pm 3.8$ days). Patients with CRC have shown the largest variation in TCP (i.e. $= 28 \pm 12.7$) with COV $\approx$ 26%. Consistently their derived α (i.e. 0.01 ± 12.7 with COV$\approx$ 50%) and α/β (i.e. 14.1 ± 8.9 with COV $\approx$ 50%) parameters have the highest variation amongst all patients. Furthermore, these results show a variation (i.e. COV $\approx$ 77%) for the derived α parameter across all cancer types.

Figure 1a–c shows the registered pre- and post-treatment FDG PET/CT images and the corresponding [^{90}Y]-microspheres VSF and TCP for a cholangiocarcinoma lesion case with complete metabolic response (CMR: 100% reduction in TLG_{liver}, i.e. lesions not visible above background at the time of follow-up). From the GLQ fit (the blue curve, $R^2 \approx 1$), the following average radiobiological parameters were derived, $T_p \approx$ 348 days, $T_k \approx 48$ days, $\alpha \approx 0.1$ Gy^{-1}, $\alpha/\beta \approx 1.5$ Gy, respectively. Furthermore, the calculated BED_∞, BED_{exp}, ΔTLG_{liver} and TCP for this case were, $\approx$ 51.3 Gy, 51.2 Gy,

Table 3 Summary of computed dosimetry

Cancer type	Dose (Gy)	BED ∞ (Gy)	BED_{exp} (Gy)	TCP (%)	ΔTLG_{liver}(%)
Breast	47.7	58.0	41.5	41.7	43.6
PNET	51.4	56.8	45.3	44.2	48.8
Adrenocortical carcinoma	52.7	67.7	26.2	17.6	23.7
CRC	127	170	90.1	65.6	75.5
Cholangiocarcinoma	28.1	46.2	46.1	50.6	56.9
CRC	33.3	37.6	6.03	0.12	−113
CRC	42.6	53.0	43.3	42.8	47.7
Rectal adenocarcinoma	12.3	12.9	12.6	20.4	25.8
Cholangiocarcinoma	34.0	51.3	51.3	82.5	98.6
CRC	33.2	37.0	8.10	0.10	−9.73
Cholangiocarcinoma	272	554	11.8	7.31	16.0
Cholangiocarcinoma	39.3	74.6	73.6	71.9	82.6
Sigmoid adenocarcinoma	53.0	62.7	61.9	54.6	70.3
Breast	45.6	93.0	93.0	79.1	89.0
Prostate	62.6	107	107	82.0	96.0
mCRC	29.5	34.2	32.7	32.1	37.5
PNET	42.2	60.9	60.7	50.8	57.0
PDAC	8.84	47.8	47.8	45.0	58.3
SBNET	231	368	368	81.3	85.1
Mesothelioma	59.9	62.5	69.9	60.6	65.7
PNET	97.8	116	116	72.8	80.3
HCC	80.6	134	12.5	0.27	0.15
Oesophageal	37.7	63.6	63.5	51.7	62.0
SBNET	50.0	55.1	40.3	31.5	35.0
NEC	17.1	21.9	10.5	0.32	−2.29

ΔTLG_{liver}, the total liver lesion glycolysis.

Table 4 Summary of the mean radiobiological parameters for patients with specific cancer type

Cancer type	T_t (days)	T_p (days)	T_k (days)	α (Gy^{-1})	α/β (Gy)	BED (Gy)	TCP (%)	ΔTLG_{liver}(%)
Breast	52.0 ± 3.0 COV ≈ 6%	152 ± 28 COV ≈ 18%	39.1 ± 15.9 COV ≈ 41%	0.045 ± 0.036 COV ≈ 80%	3.0 ± 2.0 COV ≈ 67%	67.2 ± 25.8 COV ≈ 38%	60.4 ± 18.7 COV ≈ 31%	66.3 ± 22.3 COV ≈ 34%
NET	45.3 ± 5.1 COV ≈ 11%	162 ± 33 COV ≈ 20%	32.1 ± 9.5 COV ≈ 30%	0.33 ± 0.18 COV ≈ 55%	7.87 ± 2.0 COV ≈ 25%	106.7 ± 54.1 COV ≈ 51%	46.8 ± 12.0 COV ≈ 26%	50.7 ± 13.1 COV ≈ 26%
CRC	49.4 ± 2.4 COV ≈ 5%	129 ± 19 COV ≈15%	23.5 ± 8.3 COV ≈ 35%	0.010 ± 0.005 COV ≈ 50%	14.1 ± 8.9 COV ≈ 63%	36.0 ± 15.3 COV ≈ 43%	28.2 ± 12.7 COV ≈ 45%	7.7 ± 33.1 COV ≈ 430%
Cholangiocarcinoma	46.3 ± 1.4 COV ≈ 3%	236 ± 67.2 COV ≈ 28%	28.3 ± 10.5 COV ≈ 37%	0.040 ± 0.022 COV ≈ 55%	2.38 ± 1.21 COV ≈ 51%	45.7 ± 12.8 COV ≈ 28%	53.1 ± 16.6 COV ≈ 31%	63.5 ± 18.0 COV ≈ 28%
Others	53.8 ± 3.6 COV ≈ 7%	174 ± 24 COV ≈ 14	32.2 ± 6.2 COV ≈ 19%	0.100 ± 0.040 COV ≈ 40%	4.28 ± 0.94 COV ≈ 22%	40.9 ± 11.5 COV ≈ 28%	35.3 ± 9.5 COV ≈ 27%	42.9 ± 11.0 COV ≈ 26%

COV coefficient of variance

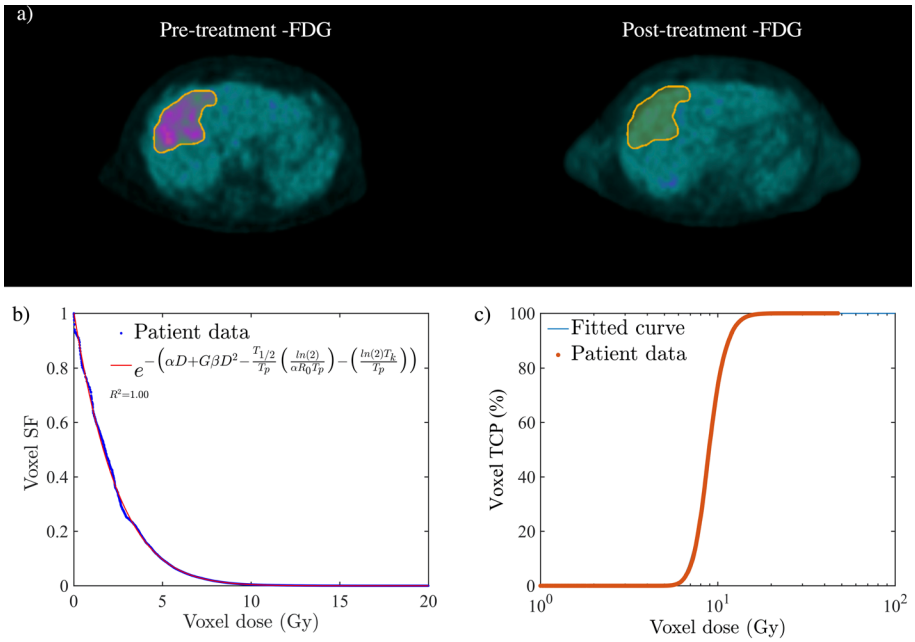

Fig. 1 Complete metabolic response (CMR) for a patient with cholangiocarcinoma liver malignancy. Deformable PET images and corresponding calculated voxel survival fraction (VSF) and tumour control probability (TCP). **a** The deformably registered pre-and post-treatment [^{18}F] FDG PET images. The registration provided a one-to-one correlation between voxels on pre-and post-treatment [^{18}F] FDG PET images. **b**, **c** The estimated voxel SF and TCP. The survival fraction and TCP were calculated based on the ^{90}Y absorbed dose and SUV volume histograms. The radiobiological parameters were derived from the generalised linear–quadratic (GLQ) fit (see Table 1)

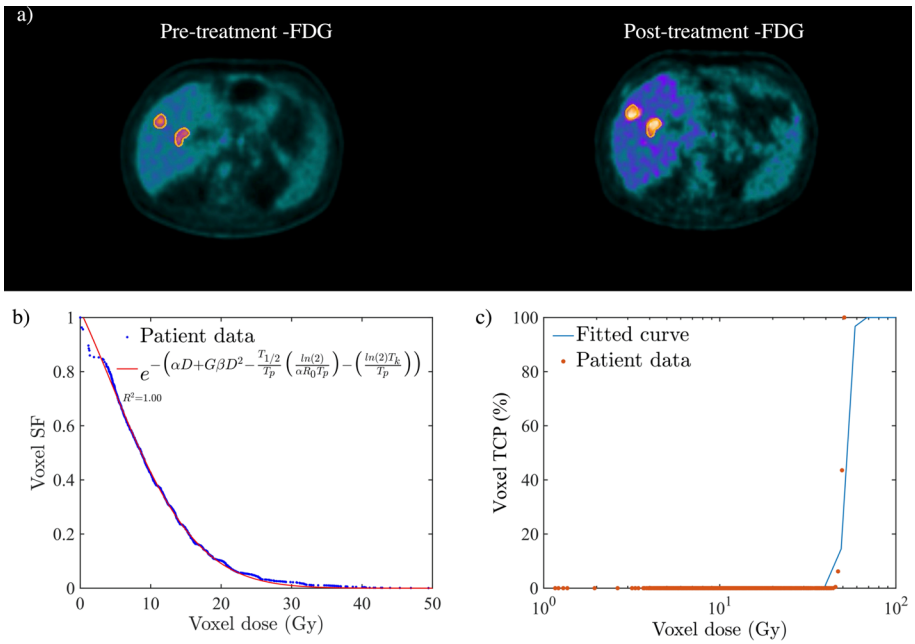

Fig. 2 Progressive metabolic disease (PMD) for a patient with metastatic CRC liver malignancy. Deformable PET images and corresponding calculated voxel SF and TCP. **a** The deformably registered pre- and post-treatment [^{18}F] FDG PET images. **b**, **c** The estimated voxel SF and TCP. The survival fraction and TCP were calculated based on the ^{90}Y absorbed dose and SUV volume histograms. The radiobiological parameters were derived from the GLQ fit (see Table 1)

99% and 83%, respectively. Figure 2a–c also shows the pre- and post-treatment FDG PET/CT images for a patient with mCRC liver lesion with progressive metabolic disease (PMD: more than a 50% increase in TLG_{liver}, $\Delta TLG_{liver} > -50\%$). In comparison to the previous case, the GLQ fit (the blue curve, $R^2 \approx 1$) for this case has shown a much shorter repopulation and kick-off time (i.e. $T_p \approx$ 108 days, $T_k \approx$ 2 days, respectively) and thus indicating a more proliferating tumour. The BED_{∞}, BED_{exp}, TCP and ΔTLG_{liver} for this case were calculated to be $\approx$ 37.2 Gy, 6.0 Gy, 0.12% and -112.7%, respectively.

The effect of tumour cell heterogeneity on the voxel SF and TCP is shown in Fig. 3a–b. Figure 3a demonstrates the pre-treatment [^{18}F] FDG PET scan for a patient with two metastatic CRC liver lesions ($L1$ and $L2$) in the left and right lobes, respectively. Both lesions (with volumes $L1 \approx 79$ mL and $L2 \approx 105$ mL) have received an average ^{90}Y dose of $\approx$ 30 Gy and the voxel SF with the GLQ fit is demonstrated in Fig. 3b. Although, the derived α parameter for both lesions ≈ 0.03 Gy^{-1}, $L1$ was shown to have a shorter T_p and T_k ($\approx$ 92 and 13 days, respectively) in comparison to $L2$ ($\approx$ 179 and 36 days). Moreover, Fig. 3c shows the calculated TCP ($\approx$ 21%) for $L2$ was $\approx$ 43% higher than the $L1$ TCP ($\approx$

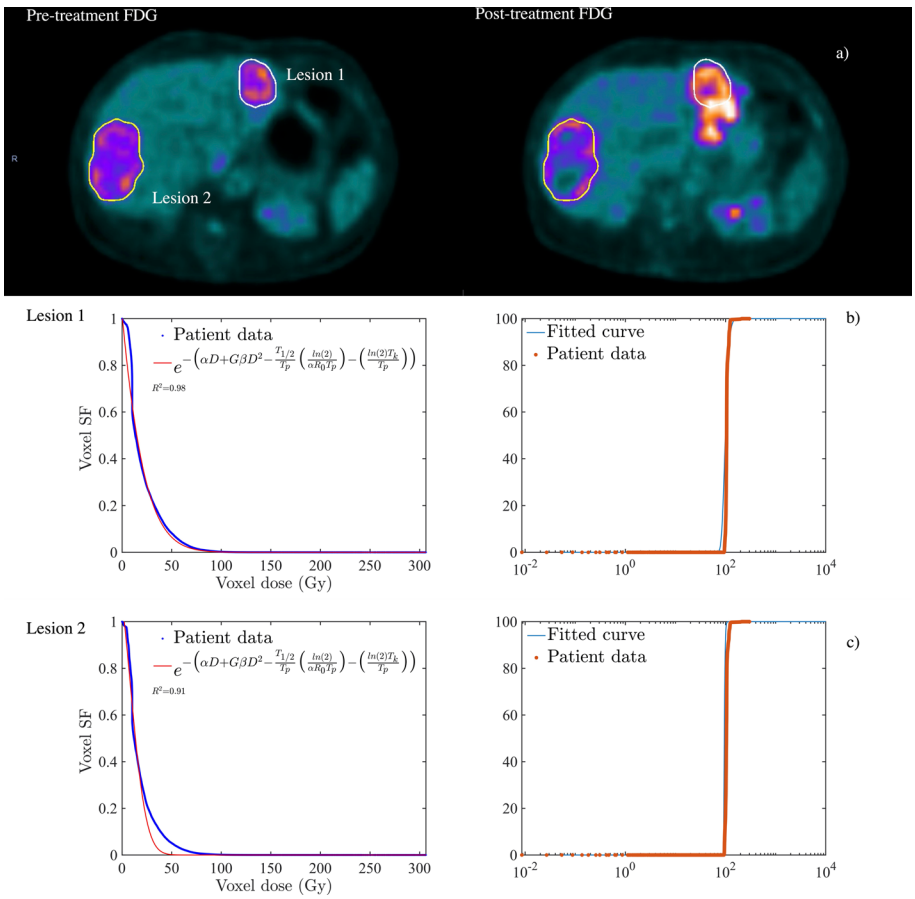

Fig. 3 Tumour cell heterogeneity within the metastatic CRC liver malignancy. **a** The deformably registered pre- and post-treatment [^{18}F] FDG PET images with two lesions on the right and left lobes are shown with the white contours. **b**, **c** The estimated voxel SF and TCP for both lesions. The survival fraction and TCP were calculated based on the ^{90}Y absorbed dose and SUV volume histograms. The radiobiological parameters were derived from the GLQ fit for each individual lesion

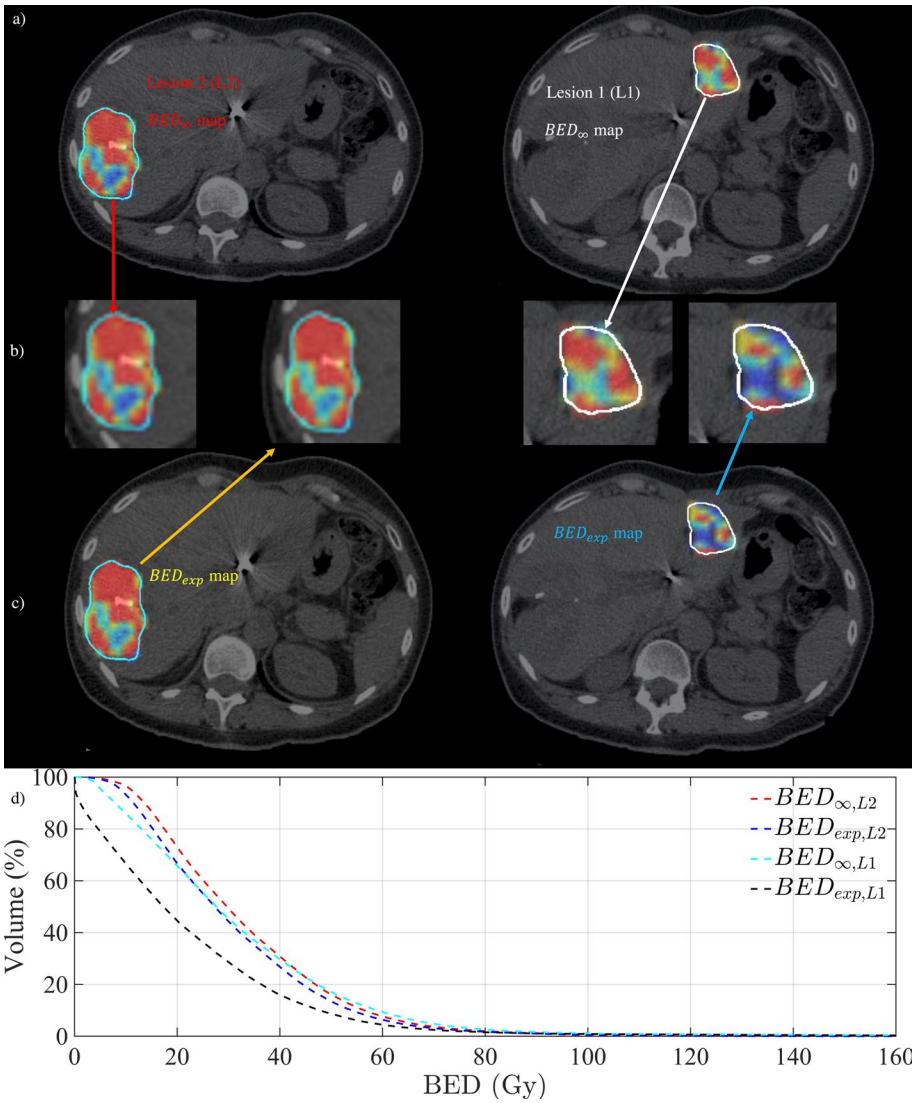

Fig. 4 The BED map for lesions shown in Fig. 3. **a**–**c** The BED_∞ and BED_{exp} maps for lesion 1 (*L*1) and lesion 2 (*L*2) with the zoom-in of the lesion BED maps. **d** The BED_∞ and BED_{exp} volume histograms for both lesions

12%). The TCP results were consistent with the ΔTLG_{liver} ($L1 \approx 14\%$ and $L2 \approx 22\%$) and BED_{exp} calculations which are shown in Fig. 4a–c.

Figure 4a–c demonstrates the BED_∞ and BED_{exp} maps for both $L1$ and $L2$ with their corresponding BED volume histograms shown in Fig. 4d, respectively. While $L2$ has a similar BED_∞ and BED_{exp} value ($\approx$ 31 and 33 Gy, respectively), the $L1$ BED_∞($\approx$ 32 Gy) was 30% higher than BED_{exp} ($\approx$ 22 Gy).

Figure 5a demonstrates a 4D plot of the theoretical T_{critic} spectrum calculated for a range of α (10^{-3}–1 Gy^{-1}), T_p(1–350 days) and R_0 ($\approx$ 1 μGy/day–100 Gy/day). ^{90}Y requires approximately 27 days (e.g. 10 half-lives, ^{90}Y half-life is $\approx$ 2.7 days) to deliver more than 98% of a targeted dose. Therefore, for ^{90}Y-SIRT, a treatment with a T_{critic} less than 27 days will be biologically less effective [23]. The black-red shaded area of the spectrum represents the most inefficient treatment (for low dose rates $\approx$ 1 μGy/day–1 Gy/day) cases

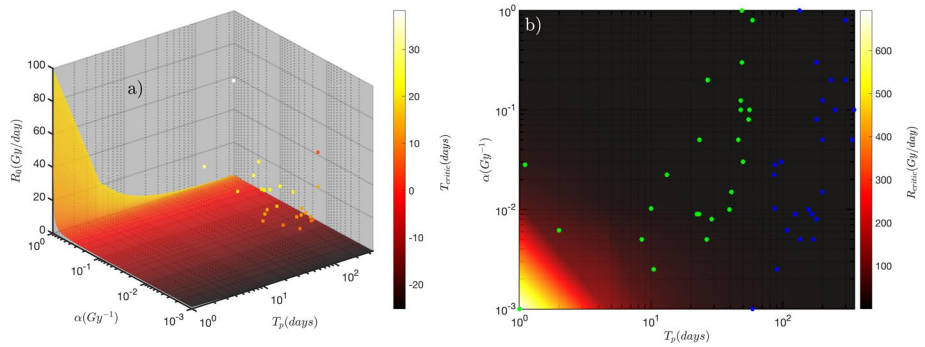

Fig. 5 The estimated critical time (T_{critic}) and dose rate (R_{critic}). **a** The four-dimensional (4D) theoretical T_{critic} spectrum and the estimated clinical T_{critic} (dot points) using the radiobiological parameters derived from patient data. **b** The theoretical R_{critic} spectrum and the estimated clinical R_{critic} and $R_{\text{critic}(k)}$ (blue and green dot points, respectively) using the radiobiological parameters derived from patient data (see Table 1). The clinical R_{critic} and $R_{\text{critic }(k)}$ were estimated using the derived repopulation T_{p} and for when $T_{\text{p}} = T_{\text{k}}$, respectively. The T_{critic} and R_{critic} spectra are predicted by Eqs. 6 and 7 for a range of α, T_{p} and initial dose rate, R_0 parameters

for different combination of α and T_p parameters and thus resulting in the shortest critical time ranging between ≈ -25 and 0 days (the negative T_{critic} means no therapeutic effect). Moreover, the spectrum shows that as the initial dose rate increases, the critical times also is prolonged (the yellow-white shaded area) and therefore suggesting a better therapeutic effect could be achieved at higher dose rates. However, the spectrum also shows that for slow proliferating (i.e. longer T_{p}, $\approx > 100$ days) and radiosensitive lesions (*e.g.* larger α parameters), even at lower initial dose rates (*e.g.* 1 Gy/day), the T_{critic} could be as high as ≈ 20 days. Furthermore, the estimated clinical critical times have shown a similar trend to the theoretically calculated T_{critic} spectrum. Patients with slow proliferating and radiosensitive lesions have shown to have higher T_{critic} compared to other patients.

Furthermore, Fig. 5b demonstrates a 3D plot of the R_{critic} spectrum calculated theoretically considering a range of α (10^{-3}–10^{0} Gy^{-1}) and T_p(1–350 days) parameters. The R_{critic} and $R_{\text{critic }(k)}$ calculated using the derived clinical radiobiological parameters were shown with blue and green markers, respectively. The theoretical spectrum has shown, lesions with larger α and longer T_{p} (black shaded area) has a higher R_{critic}. This region can represent lesions with low to medium radioresistivity. However, smaller R_{critic} was predicted for lesions with smaller α and shorter T_p (yellow-white shaded area). Most of the clinical R_{critic} was calculated to be within black shaded area (i.e. $\approx$ 0.003–12 Gy/day). However, there is an evident shift towards a higher critical dose rate (the yellow-white shaded area) when the clinically driven T_{k} was assumed to be the new T_{p} (as it was explained in the method section, as $T_p \rightarrow T_{\text{k}}$ represents the highest acceleration in tumour proliferation rate scenario).

Sub-figures in Fig. 6a–e are 3D plots which demonstrate the relationship between the clinically driven radiobiological parameters and calculated TCP. Figure 6a shows that lower and higher TCPs were achieved for radioresistant (i.e. small α parameter) and radiosensitive (i.e. large α parameter) lesions, respectively. Also, it shows that radioresistant and radiosensitive lesions tend to have a shorter and longer T_{k}, respectively. Figure 6b also shows that highly proliferating lesions (i.e. short T_{p}) have a shorter T_k and

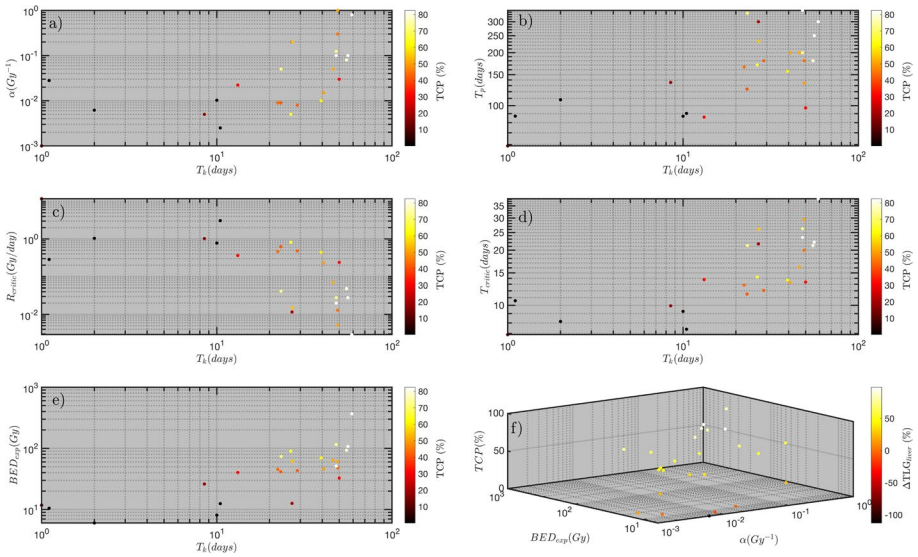

Fig. 6 **a**–**e** The relationship between the clinically estimated radiobiological parameters and TCP. **f** 4D scatter plot demonstrating the relationship between the biological effective dose (BED_{exp}), α parameter, TCP, and the total liver lesion glycolysis ΔTLG_{liver}

therefore they resulted in a higher R_{critic} (shown in Fig. 6c) and lower TCP. Furthermore, in Fig. 6d, e, lesions with shorter T_k have shown to have the lowest T_{critic} and thus lowest BED_{exp} and TCP. Figure 6f is a 4D plot comparing the BED_{exp}, TCP and ΔTLG_{liver} for lesions with different α parameters. Lesions with smaller α values have shown to result in lower TCP and ΔTLG_{liver}.

Discussion

The value of functional images for personalised therapy and dosimetry of ^{90}Y-SIRT is limited by cancer histological and genomic heterogeneity [42, 43]. This is further compounded by the limited knowledge of the clinically relevant radiobiological parameters to evaluate the biological effectiveness of the ^{90}Y-SIRT. However, many clinical studies have shown that the GLQ model can demonstrate the relationship between the radiation absorbed dose to cell killing and it has achieved great success in helping researchers and clinicians to investigate response to radiation and interpret clinical outcome data, design new treatment strategies, and compare different radiation modalities [19, 23, 44–46]. The fundamental principle of the GLQ model takes account of two main cellular damages: lethal (DNA DSBs), and sub-lethal (DNA single-strand breaks, SSBs) and their repair mechanism. Furthermore, results presented in this study have shown that the GLQ model can be used to derive the clinically relevant radiobiological parameters and they can be utilised to personalise ^{90}Y-SIRT dosimetry.

Four radiobiological parameters, T_p, T_k, α, α/β were derived for twenty-five patients with liver malignancy. One of the main results of this analysis is that the T_p, or proliferation rate of tumours, is a very influential parameter affecting the BED and treatment outcome (e.g. TCP). The tumour T_p was initially reported as a tool to estimate the rate of growth of pulmonary metastases from colorectal cancer [47]. Additionally, T_p can be calculated based on preoperative standard diagnostic techniques and has been shown

to describe the tumour biological aggressiveness of a neoplasm [48–50]. In this study it was predicted that patients with mCRC liver lesions have shortest T_p with mean of $\approx 129 \pm 19$ days. This is within the range of T_p measured in vivo (i.e. mean of ≈ 92 [51] and 150 [52]days). One previous study [51] has shown that the T_p of hepatic metastases in patients with CRC may be a useful prognostic marker. This clinical study suggested that patients with a tumour T_p of less than 92.4 days have a poor prognosis in comparison to patients who had tumour with T_p of greater than 92.4 days. Furthermore, it was indicated that patients with tumours that have shorter T_p carrying a greater risk of residual primary cancer in the abdominal cavity [51]. This is also consistent with the results presented in our current study. Amongst patients who had mCRC, patients with shorter T_p have shown the worst TCP and metabolic response from ΔTLG_{liver} (e.g. $T_p \approx 87$ days, TCP = 0.1% and $\Delta TLG_{liver} = -9.7\%$). Furthermore, the large variation in the α parameter for CRC patients indicates a significant variation in the type of tumour within the patients. This explains why we have also seen a larger variation in the treatment outcome for these patients. Therefore, these results suggest for an optimal and personalised treatment; it is very critical to prescribe the dose based on clinically derived radiobiological parameters.

Patients with cholangiocarcinoma have been found to have the longest $T_p \approx 236 \pm 62.7$ days ($\approx$ 59–336 days). This is also within the range of a previously published clinical study [53] which found a similar range for the cholangiocarcinoma tumours $T_p \approx$ 14.5–513 days. In comparison to CRC, NET, breast, and the other cancer types, on average cholangiocarcinoma tumours are shown to have best TCP ($53\% \pm 17\%$) and ΔTLG_{liver} ($63\% \pm 18\%$) response, and they have the second shortest T_k (28 ± 10 days). This suggests that the radiation treatment response for tumours with long T_p are less influenced by the T_k parameter. This is also valid for all the cancer types investigated in this study, and the general relationship between T_k and T_p parameters is presented in Fig. 6b. The trend of these data has shown that tumours with longer T_p will have a longer T_k and higher TCP.

The time factors (T_p, T_k, T_{critic} and treatment time) are amongst the key elements in radiation oncology [54]. Furthermore, the importance of delays during a course of radiotherapy or relatively low dose rate RNT (compared to EBRT) with long treatment time has been investigated in recent decades, and different recommendations on the delay-compensation options have been published [24, 27]. Fast tumour cell repopulation has been suggested as the main reason why prolonging overall treatment time in EBRT or RNT reduces the therapeutic efficacy and thus the TCP and overall survival in many human tumours [55]. In our previous study we have shown that the T_{critic} could be considered as another prognostic marker [23]. The T_{critic} accounts for two radiobiological parameters, T_p and α and it considers the initial dose rate for a particular treatment. Results presented in Table 2 and Fig. 5a have shown, generally, that tumours with short T_p and small α parameters have the shortest T_{critic} and thus largest R_{critic}. The relationship between these radiobiological parameters and quantities for all twenty-five patients is presented in Fig. 6c–d. The trend of both data showed that, regardless of cancer type, tumours with larger T_p and consequently T_k result in shorter T_{critic} and thus larger R_{critic}. Moreover, as it was shown in Fig. 6e, the T_k has a significant impact on the BED calculation. The short T_k

means that the acceleration in proliferation rate in tumours with shorter T_k occurs at an early time point after the start of the treatment. As shown in Fig. 6d, this will result in further shortening the T_{critic} and thus reducing the therapeutic efficacy and the TCP. Therefore, these results suggest for such tumours, the ^{90}Y-SIRT will be only effective at higher initial dose rate (e.g. $R_0 > 50$ Gy/day which corresponds to the yellow-white shaded area in Fig. 5a; regions where T_{critic} is estimated to be greater than 20 days).

Furthermore, it was estimated that the values for α and α/β parameters range in $\approx 0.001–1$ Gy^{-1} and $\approx 1–49$ Gy, respectively. The average α parameters for breast, NET, CRC and cholangiocarcinoma were, 0.045 ± 0.036 Gy^{-1}, 0.331 ± 0.183 Gy^{-1}, 0.010 ± 0.005 Gy^{-1} and 0.040 ± 0.022 Gy^{-1} respectively. These values are within the range of the previously published clinical data 0.054 Gy^{-1}, 0.015 Gy^{-1}, 0.037 Gy^{-1} clinically driven for breast, CRC, and cholangiocarcinoma cancer types [16]. To the best of our knowledge, there are no published values for clinically driven α parameter for NET cancer cells. These results show that patients with metastatic CRC tumours have a consistently smaller α parameter and are the most radioresistant tumour type amongst all the other cancer types investigated in this study. As it was shown in Fig. 6a, in general tumours with smaller α parameters tend to have shorter T_k, therefore resulting in poor TCP.

The calculated ΔTLG_{liver} has shown a good correlation with TCP values. The average ΔTLG_{liver} and TCP calculated for all twenty-five patients were, $\approx 45\% \pm 9\%$ and $43 \pm 6\%$, respectively. As it was demonstrated in Fig. 6f, tumours with larger α parameters have consistently resulted in high BED_{exp}, TCP and ΔTLG_{liver}. These results suggest that ΔTLG_{liver} and TCP have a similar relationship with the driven radiobiological parameters and thus ΔTLG_{liver} could be considered as an alternative radiobiological metric to the TCP.

Finally, results from this study suggest that the standard BED formulism (i.e. BED_∞) without considering the T_p and T_k time parameters can be a misleading metric to assess the tumour radiation biological response. For example, considering the patient case presented in Fig. 4, although both liver lesions in the left and right lobes received similar average absorbed dose of ≈ 30 Gy and $BED_\infty \approx 32$ Gy, due to shorter T_p and T_k(≈ 92 and 23 days), the lesion in the left lobe ($L1$) resulted in a much lower TCP (i.e. $\approx 43\%$ less than $L2$ TCP). However, when the T_p and T_k time parameters were included in the BED calculation (i.e. BED_{exp}), while a similar BED_∞ and BED_{exp} values (≈ 31 and 33 Gy) was achieved for $L2$, the $L1$ BED_∞(≈ 32 Gy) was reduced to $BED_{exp} \approx 22$ Gy. Therefore, a better correlation between the BED and TCP was achieved.

In summary, this study demonstrates a novel approach whereby using pre- and post-treatment FDG PET/CT images, in addition to radiosensitivity of the tumour cells, valuable information on the temporal changes (such tumour T_k and T_p) in FDG uptake of tumour could be estimated. These in vivo-driven radiobiological parameters may not only lead towards personalised dosimetry in patients with liver malignancy treated with ^{90}Y-SIRT but for other targeted radionuclide therapy modalities such as Lutetium-177 therapy.

Conclusion

Results presented in this study show that ^{90}Y PET/CT with pre- and post-treatment FDG PET/CT images can be used to derive the clinically relevant radiobiological parameters (i.e. T_p, T_k, α, α/β) of the GLQ model. It was estimated that the values for α and α/β parameters range in ≈ 0.001–$1\ \mathrm{Gy}^{-1}$ and ≈ 1–49 Gy respectively. We have demonstrated that the time factors, T_p, T_k, T_{critic} are the key parameters when evaluating liver malignancy lesion response to [^{90}Y] SIR-Spheres treatment. Patients with cholangiocarcinoma have been shown to have the longest average T_p ($\approx 236 \pm 67$ d), highest TCP ($\approx 53 \pm 17\%$) and $\Delta TLG_{liver} \approx 64\%$ while patients with metastatic CRC tumours have the shortest average T_p ($\approx 129\ \mathrm{d} \pm 19$ d), lowest TCP ($\approx 28\% \pm 13\%$) and $\Delta TLG_{liver} \approx 8\%$ respectively. Therefore, these results suggest for such tumours, the ^{90}Y-SIRT will be only effective at higher initial dose rate (*e.g.* >50 Gy/day).

Abbreviations

BED	Biological effective dose
CMR	Complete metabolic response
COV	Coefficient of variation
CRC	Colorectal cancer
CT	Computed tomography
DVH	Dose volume histogram
DSB	DNA double-strand break
EBRT	External beam radiotherapy
GLQ	Generalised linear–quadratic
HCC	Hepatocellular carcinoma
L	Lesion
mCRC	Metastatic colorectal cancer
NEC	Neuroendocrine carcinoma
PDAC	Pancreatic ductal adenocarcinoma
PET	Positron emission tomography
PMD	Progressive metabolic disease
PNET	Pancreatic neuroendocrine tumours
RNT	Radionuclide therapy
SBNET	Small bowel neuroendocrine tumours
SF	Survival fraction
SSB	DNA single-strand break
SUV	Standardised uptake value
SIRT	Selective internal radionuclide therapy
SPECT	Single-photon emission computed tomography
TLG	Total liver lesion glycolysis
TCP	Tumour control probability
VSF	Voxel survival fraction

Acknowledgements

We gratefully acknowledge the generous support from the Varian development team, especially George Andl and Johnny Cheng.

Author contributions

YG led the study design, performed data analysis, and was the primary manuscript producer. KW aided in study design and manuscript production. DB facilitated overall study concept and design, advised on data analysis techniques, and aided in manuscript preparation. All authors read and approved the final manuscript.

Funding

YG is funded by a Varian Research Collaboration Grant.

Availability of data and materials

Data are available upon reasonable request subject to ethical approval.

Declarations

Ethics approval and consent to participate

Written informed consent to use all subject clinical and imaging data was provided by the participants when they agreed to undergo the interventional procedure.

Consent for publication
Not applicable.

Competing interests
None.

Received: 17 January 2022 Accepted: 20 July 2022
Published online: 30 July 2022

References

1. Tsang ES, et al. Efficacy and prognostic factors for Y-90 radioembolization (Y-90) in metastatic neuroendocrine tumors with liver metastases. Can J Gastroenterol Hepatol. 2020;2020:5104082.
2. Hendlisz A, et al. Phase III trial comparing protracted intravenous fluorouracil infusion alone or with yttrium-90 resin microspheres radioembolization for liver-limited metastatic colorectal cancer refractory to standard chemotherapy. J Clin Oncol Off J Am Soc Clin Oncol. 2010;28:3687–94.
3. Levillain H, et al. International recommendations for personalised selective internal radiation therapy of primary and metastatic liver diseases with yttrium-90 resin microspheres. Eur J Nucl Med Mol Imaging. 2021;48:1570–84.
4. Vilgrain V, et al. Efficacy and safety of selective internal radiotherapy with yttrium-90 resin microspheres compared with sorafenib in locally advanced and inoperable hepatocellular carcinoma (SARAH): an open-label randomised controlled phase 3 trial. Lancet Oncol. 2017;18:1624–36.
5. Chow PKH, et al. SIRveNIB: selective Internal radiation therapy versus sorafenib in Asia-Pacific patients with hepatocellular carcinoma. J Clin Oncol Off J Am Soc Clin Oncol. 2018;36:1913–21.
6. Ricke J, et al. Impact of combined selective internal radiation therapy and sorafenib on survival in advanced hepatocellular carcinoma. J Hepatol. 2019;71:1164–74.
7. Zhen Y, et al. A pooled analysis of transarterial radioembolization with yttrium-90 microspheres for the treatment of unresectable intrahepatic cholangiocarcinoma. OncoTargets Ther. 2019;12:4489–98.
8. Levillain H, et al. Personalised radioembolization improves outcomes in refractory intra-hepatic cholangiocarcinoma: a multicenter study. Eur J Nucl Med Mol Imaging. 2019;46:2270–9.
9. Gangi A, et al. Intrahepatic cholangiocarcinoma treated with transarterial Yttrium-90 Glass microsphere radioembolization: results of a single institution retrospective study. J Vasc Interv Radiol JVIR. 2018;29:1101–8.
10. Roncali E, Taebi A, Foster C, Vu CT. Personalized dosimetry for liver cancer Y-90 radioembolization using computational fluid dynamics and monte carlo simulation. Ann Biomed Eng. 2020;48:1499–510.
11. Willowson KP, Tapner M, Bailey DL. A multicentre comparison of quantitative 90Y PET/CT for dosimetric purposes after radioembolization with resin microspheres. Eur J Nucl Med Mol Imaging. 2015;42:1202–22.
12. Song YS, et al. PET/CT-based dosimetry in 90Y-microsphere selective internal radiation therapy: single cohort comparison with pretreatment planning on 99mTc-MAA imaging and correlation with treatment efficacy. Medicine (Baltimore). 2015;94:e945.
13. Brosch J, et al. 3D image-based dosimetry for Yttrium-90 radioembolization of hepatocellular carcinoma: impact of imaging method on absorbed dose estimates. Phys Med. 2020;80:317–26.
14. Kao YH, Tan EH, Ng CE, Goh SW. Yttrium-90 time-of-flight PET/CT is superior to bremsstrahlung SPECT/CT for postradioembolization imaging of microsphere biodistribution. Clin Nucl Med. 2011;36:e186-187.
15. Kirsch DG, et al. The future of radiobiology. JNCI J Natl Cancer Inst. 2017;110:329–40.
16. van Leeuwen CM, et al. The alfa and beta of tumours: a review of parameters of the linear–quadratic model, derived from clinical radiotherapy studies. Radiat Oncol. 2018;13:96.
17. Jones L, Hoban P, Metcalfe P. The use of the linear quadratic model in radiotherapy: a review. Australas Phys Eng Sci Med. 2001;24:132–46.
18. Brenner DJ. Point: the linear–quadratic model is an appropriate methodology for determining iso-effective doses at large doses per fraction. Semin Radiat Oncol. 2008;18:234–9.
19. Wang JZ, Huang Z, Lo SS, Yuh WTC, Mayr NA. A generalized linear–quadratic model for radiosurgery, stereotactic body radiation therapy, and high-dose rate brachytherapy. Sci Transl Med. 2010;2:39ra48.
20. Huang Z, et al. A generalized linear–quadratic model incorporating reciprocal time pattern of radiation damage repair. Med Phys. 2012;39:224–30.
21. McMahon SJ. The linear quadratic model: usage, interpretation and challenges. Phys Med Biol. 2018;64:01TR01.
22. Willowson KP, et al. Clinical and imaging-based prognostic factors in radioembolisation of liver metastases from colorectal cancer: a retrospective exploratory analysis. EJNMMI Res. 2017;7:46.
23. Gholami YH, et al. Comparison of radiobiological parameters for 90Y radionuclide therapy (RNT) and external beam radiotherapy (EBRT) in vitro. EJNMMI Phys. 2018;5:18.
24. Dale RG, et al. Practical methods for compensating for missed treatment days in radiotherapy, with particular reference to head and neck schedules. Clin Oncol R Coll Radiol G B. 2002;14:382–93.
25. Allen B, Loredana M, Bezak E. Biomedical physics in radiotherapy for cancer. (CSIRO Publishing, 2012). https://doi.org/10.1071/9780643103306.
26. González Ferreira JA, Jaén Olasolo J, Azinovic I, Jeremic B. Effect of radiotherapy delay in overall treatment time on local control and survival in head and neck cancer: review of the literature. Rep Pract Oncol Radiother. 2015;20:328–39.
27. Hendry JH, et al. A modelled comparison of the effects of using different ways to compensate for missed treatment days in radiotherapy. Clin Oncol R Coll Radiol G B. 1996;8:297–307.
28. Bese NS, Hendry J, Jeremic B. Effects of prolongation of overall treatment time due to unplanned interruptions during radiotherapy of different tumor sites and practical methods for compensation. Int J Radiat Oncol Biol Phys. 2007;68:654–61.

29. Tai A, Erickson B, Khater KA, Li XA. Estimate of radiobiologic parameters from clinical data for biologically based treatment planning for liver irradiation. Int J Radiat Oncol Biol Phys. 2008;70:900–7.
30. Pacilio M, et al. Differences in 3D dose distributions due to calculation method of voxel *S*-values and the influence of image blurring in SPECT. Phys Med Biol. 2015;60:1945–64.
31. Chiesa C, et al. Radioembolization of hepatocarcinoma with 90Y glass microspheres: development of an individualized treatment planning strategy based on dosimetry and radiobiology. Eur J Nucl Med Mol Imaging. 2015;42:1718–38.
32. Potrebko PS, et al. SPECT/CT image-based dosimetry for Yttrium-90 radionuclide therapy: application to treatment response. J Appl Clin Med Phys. 2018;19:435–43.
33. Kadoya N, et al. Evaluation of various deformable image registration algorithms for thoracic images. J Radiat Res (Tokyo). 2014;55:175–82.
34. Weisenthal LM, Lippman ME. Clonogenic and nonclonogenic in vitro chemosensitivity assays. Cancer Treat Rep. 1985;69:615–32.
35. Shoemaker RH, et al. Application of a human tumor colony-forming assay to new drug screening. Cancer Res. 1985;45:2145–53.
36. Croteau E, et al. PET metabolic biomarkers for cancer. Biomark Cancer. 2016;8:61–9.
37. Zhu A, Lee D, Shim H. Metabolic pet imaging in cancer detection and therapy response. Semin Oncol. 2011;38:55–69.
38. Yan D, et al. Tumor voxel dose-response matrix and dose prescription function derived using 18F-FDG PET/CT images for adaptive dose painting by number. Int J Radiat Oncol Biol Phys. 2019;104:207–18.
39. Baechler S, Hobbs RF, Prideaux AR, Wahl RL, Sgouros G. Extension of the biological effective dose to the MIRD schema and possible implications in radionuclide therapy dosimetry. Med Phys. 2008;35:1123–34.
40. World Congress of Medical Physics and Biomedical Engineering 2006: August 27–Septmber 1, 20006 COEX Seoul, Korea. Springer-Verlag; 2007. https://doi.org/10.1007/978-3-540-36841-0.
41. Li XA, Wang JZ, Stewart RD, DiBiase SJ. Dose escalation in permanent brachytherapy for prostate cancer: dosimetric and biological considerations. Phys Med Biol. 2003;48:2753–65.
42. Gerlinger M, et al. Intratumor heterogeneity and branched evolution revealed by multiregion sequencing. N Engl J Med. 2012;366:883–92.
43. Fleuren GJ, Gorter A, Kuppen PJ, Litvinov S, Warnaar SO. Tumor heterogeneity and immunotherapy of cancer. Immunol Rev. 1995;145:91–122.
44. Kirkpatrick JP, Meyer JJ, Marks LB. The linear–quadratic model is inappropriate to model high dose per fraction effects in radiosurgery. Semin Radiat Oncol. 2008;18:240–3.
45. Brenner DJ. The linear–quadratic model is an appropriate methodology for determining isoeffective doses at large doses per fraction. Semin Radiat Oncol. 2008;18:234–9.
46. Sachs RK, Hahnfeld P, Brenner DJ. The link between low-LET dose-response relations and the underlying kinetics of damage production/repair/misrepair. Int J Radiat Biol. 1997;72:351–74.
47. Collins VP, Loeffler RK, Tivey H. Observations on growth rates of human tumors. Am J Roentgenol Radium Ther Nucl Med. 1956;76:988–1000.
48. Schwartz M. A biomathematical approach to clinical tumor growth. Cancer. 1961;14:1272–94.
49. Spratt JS, Meyer JS, Spratt JA. Rates of growth of human neoplasms: part II. J Surg Oncol. 1996;61:68–83.
50. Cucchetti A, et al. Tumor doubling time predicts recurrence after surgery and describes the histological pattern of hepatocellular carcinoma on cirrhosis. J Hepatol. 2005;43:310–6.
51. Nomura K, et al. Relationship between doubling time of liver metastases from colorectal carcinoma and residual primary cancer. Dig Surg. 1998;15:21–4.
52. Burke JR, et al. Tumour growth rate of carcinoma of the colon and rectum: retrospective cohort study. BJS Open. 2020;4:1200–7.
53. De Rose AM, et al. Prognostic significance of tumor doubling time in mass-forming type cholangiocarcinoma. J Gastrointest Surg Off J Soc Surg Aliment Tract. 2013;17:739–47.
54. Hall EJ. Time dose and fractionation in radiotherapy. A comparison of two evaluation systems in clinical use. Br J Radiol. 1969;42:427–31.
55. Tubiana M. Repopulation in human tumors. A biological background for fractionation in radiotherapy. Acta Oncol Stockh Swed. 1988;27:83–8.

Publisher's Note